ELSEVIER

Chemical Engineering Journal 132 (2007) 215–225

Chemical Engineering Journal

www.elsevier.com/locate/cej

Determination of ozone mass transfer coefficient in a tall continuous flow counter-current bubble contactor

Gunjan Tiwari, Purnendu Bose *

Environmental Engineering and Management Programme, Department of Civil Engineering, Indian Institute of Technology Kanpur, Kanpur 208016, India

Received 27 March 2006; received in revised form 18 December 2006; accepted 19 December 2006

Abstract

Preliminary experiments in a continuous flow counter-current bubble type ozone contactor, 3 m in length and 25 mm diameter, indicated that the gas phase hold-up (ε_G) in the contactor increased linearly from 8 to 15% when gas flow rate (Q_g) was increased from 500 to 1000 mL min^{-1} (8.33×10^{-6} to 1.67×10^{-5} m^3 s^{-1}). The liquid phase dispersion coefficient (D_L) in the contactor increased from $(2.02 \pm 0.83) \times 10^{-3}$ to $(2.34 \pm 0.46) \times 10^{-3}$ m^2 s^{-1} when Q_g was increased from 500 to 1000 mL min^{-1} (8.33×10^{-6} to 1.67×10^{-5} m^3 s^{-1}). The contactor was mathematically modeled considering the hydrostatic pressure variation along reactor height, and assuming the gas and liquid phases in the reactor to be plug flow and mixed flow, respectively. Using this model, aqueous ozone concentration was simulated at various reactor heights as a function of time. The simulation results using an ozone mass transfer coefficient (K_La) of 0.025 s^{-1} matched well with the corresponding experimental data. Experimental data on gaseous ozone concentration effluent from the reactor was also obtained as a function of time. This data also matched well with corresponding simulation results for a K_La value of 0.025 s^{-1}. Sensitivity analysis indicated that the model simulation results were relatively insensitive to changes in K_La value in the range of 0.015–0.035 s^{-1}. The work described in this paper is the first part of a continuing study to develop a fully mechanistic model of a tall ozone contactor for degradation of micro-pollutants in water.

Keywords: Ozone; Contactor; Mass transfer coefficient; Model

1. Introduction

Modeling of tall bubble type ozone contactors involves providing mathematical description of the system, including specification of the reactor type (i.e., semi-batch or continuous flow), reactor dimensions and mode of contact of liquid and gaseous phases (i.e., co-current or counter-current). Ozone mass transfer, ozone self-decomposition in liquid and gaseous phases and ozone consumption by substrates in the liquid phase must also be specified. Ozone transfer efficiency from gas to liquid phase is mainly controlled by physical parameters such as temperature, gas flow rate, ozone partial pressure, and reactor geometry [1,2]. Chemical parameters such as pH, ionic strength and composition of aqueous solution also affect ozone transfer [1]. The effect of physical parameters can be adequately represented by a partition coefficient, e.g., Henry's coefficient, for describing ozone distribution between gas and liquid phase, and a mass transfer coefficient [3]. The effect of chemical parameters can be represented by an adequate description of ozone decomposition and consumption in the aqueous phase [2].

Development and validation of fully mechanistic models for ozone contactors as described above is an important and evolving area of research. It involves various steps, first being the fabrication and characterization of the contactor. This is followed by utilization of the experimental data obtained during the ozone contactor operation under various conditions to test models of ozone decomposition and degradation of micro-pollutants in pure waters, or in waters containing background organic and inorganic impurities.

Reactor characterization include determination of gas phase hold-up (ε_g), liquid phase dispersion coefficient (D_L), and ozone mass transfer coefficient (K_La). A large number of studies have been carried out concerning characterization of ozone contactors [4–15]. These studies resulted in better understanding of ozone contactor characteristics and, in many cases, led to the development of regression equations relating the above parameters to reactor operation conditions, i.e., temperature, gas and liquid flow rates, etc. Based on the above characterizations,

* Corresponding author. Tel.: +91 512 2597403; fax: +91 512 2597395.
E-mail address: pbose@iitk.ac.in (P. Bose).

1385-8947/$ – see front matter © 2007 Elsevier B.V. All rights reserved.
doi:10.1016/j.cej.2006.12.025

Nomenclature

A	column cross-section area (m^2)
D_L	liquid dispersion coefficient ($m^2\ s^{-1}$)
g	acceleration due to gravity ($m\ s^{-2}$)
H	height of the reactor (m)
K_La	mass transfer coefficient (s^{-1})
M_{O_2}	molecular weight of oxygen ($g\ mol^{-1}$)
M_{O_3}	molecular weight of ozone ($g\ mol^{-1}$)
$[O_2]_g$	gas phase oxygen concentration ($g\ m^{-3}$)
$[O_3]_g$	gas phase ozone concentration ($g\ m^{-3}$)
$[O_3]_l$	aqueous phase ozone concentration ($g\ m^{-3}$)
$[O_3]_g^o$	influent gaseous ozone concentration ($g\ m^{-3}$)
$[O_3]_l^s$	saturated aqueous phase ozone concentration corresponding to $[O_3]_g$ ($g\ m^{-3}$)
P	total pressure (Pa)
P_A	atmospheric pressure (Pa)
P_{O_2}	partial pressure of oxygen in the column (Pa)
P_{O_3}	partial pressure of ozone (Pa)
P^o	total pressure at $x=0$ (Pa)
$P_{O_3}^o$	partial pressure of ozone at $x=0$ (Pa)
Q_g	gas flow rate at $x=0$ at STP ($m^3\ s^{-1}$)
Q_{go}	gas flow rate at $x=0$ at the prevalent pressure ($m^3\ s^{-1}$)
Q_l	liquid flow rate ($m^3\ s^{-1}$)
R	universal gas constant ($J\ mol^{-1}\ K^{-1}$)
R_{O_3}	net rate of ozone mass transfer from gas to liquid phase ($g\ m^{-3}\ s^{-1}$)
S	solubility ratio ($M\ M^{-1}$)
t	time after start of ozonation (s)
T	temperature (K)
U_g	superficial gas velocity at any height at the prevalent pressure ($m\ s^{-1}$)
U_{go}	superficial gas velocity at the prevalent pressure at $x=0$, $U_{go}=Q_{go}/A$ ($m\ s^{-1}$)
U_G	superficial gas velocity at STP at $x=0$, $U_G=Q_g/A$ ($m\ s^{-1}$)
U_l	superficial liquid velocity ($m\ s^{-1}$)
V	volume of reactor (m^3)
x	distance along column height, $x=0$ at the bottom (m)
y	ozone mole fraction in gas phase at any height at the prevalent pressure
y_o	ozone mole fraction in gas phase at $x=0$, at the prevalent pressure

Greek symbols

ε_g	gas hold-up
ε_l	liquid hold-up $(1-\varepsilon_g)$
ρ	density of water ($kg\ m^{-3}$)

models for continuous-flow ozone contactors describing ozone self-decomposition, and in many cases, degradation of micro-pollutants have also been formulated by several researchers [16–30].

In most studies concerning modeling of ozone contactors, the mass transfer coefficient (K_La) and other reactor characteristics are estimated from data or regression equations available in the literature. While this is quite effective in many cases, experimental determination of reactor characteristics for the specific reactor system being studied is always preferable. In this study we describe a methodology involving comparison of dynamic measurements of aqueous and gas phase ozone concentration with mechanistic model simulations to estimate K_La values in continuous bubble type counter-current ozone contactors. Some other researchers [5,12] have also demonstrated methods to estimate K_La values in ozone bubble contactors using similar principles. Thus, while the topic is not new, the methodology described in this study is novel, simpler than other existing methods, and can be easily implemented with limited experimental data to give reasonably accurate value for the mass transfer coefficient.

2. Experimental setup

The experimental apparatus consisted of the following components. A tall bubble column ozone contactor, oxygen cylinder, ozone generator, mass flow controller, peristaltic pump and gas phase ozone monitors. The ozone contactor was made of seven pre-fabricated cylindrical 'borosil' glass sections with male and female ground glass joints. Diameter of each section was about 25 mm. Each glass section was approximately 500 mm in length, and had a sampling port approximately in the middle. Five sections used in the intermediate part of the column were identical, while the bottom section was equipped with a gas inlet, liquid outlet, a liquid drain, and a porous sintered glass plate for supporting the liquid column and generation of gas bubbles. The top section had arrangements for gas outlet and liquid inlet.

The sampling port in each section was fabricated by fusing a 6 mm 'borosil' glass tube to the section. The other end of this tube was threaded, and was kept closed using 'teflon' screw cap equipped with 'teflon' coated septa. For extracting samples from a sample port, a 10 cm long and 6 mm diameter stainless-steel syringe needle with luer-lock fittings was kept permanently in place by piercing through the 'teflon' cap of the sampling port, such that the tip of the needle was at the central axis of the ozone contactor. The luer-lock connection at the other end of the needle was kept closed at all times with a 'teflon' plug. During sample collection, the plug was removed and a syringe attached to the needle. After sample collection, the syringe was disengaged, and the 'teflon' plug put back in place. The seven glass sections were attached together as shown in Fig. 1 with wire clamps at each ground glass joint. The whole setup was also tightly secured to a frame by metal clamps. The final assembled column has seven sampling ports at 0, 0.5, 1.0, 1.5, 2.0, 2.5 and 3.0 m height from the bottom.

Schematic of the experimental setup is shown in Fig. 2. Ozone was generated in gas phase by passing pure oxygen from an oxygen cylinder through an ozone generator (ANSEROS, COM-AD-04, Germany). This gas mixture was applied to the bottom of the reactor, where it bubbled through the porous ceramic plate and moved upwards through the reactor. The gas flow into the

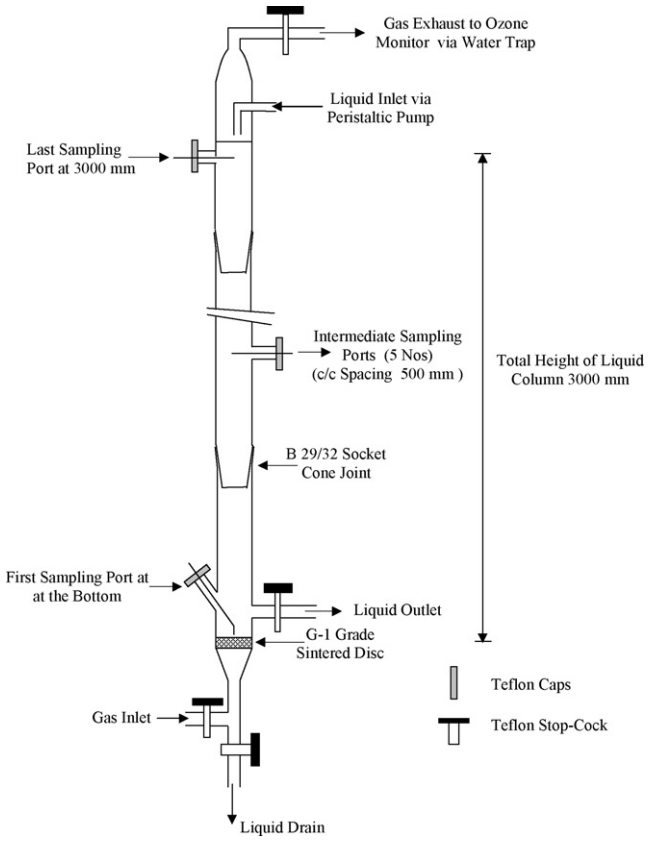

Fig. 1. Schematic of the assembled tall ozone contactor.

reactor was controlled using an on-line mass flow controller (AALBORG, GFC171S, USA). The ozone concentration in the gas influent to and effluent from the reactor was measured using online ozone monitors (ANSEROS, Ozomat GM-6000-OEM, Germany). Before entering the ozone monitor at the effluent end of the column, the effluent gas was routed through a water trap (see Fig. 2) to remove any entrained water droplets. Water was introduced into the reactor from the top using a peristaltic pump (IKA LABORTECHNIK, IKA PA MCP, Germany). Water was also extracted at the same rate from the bottom of the reactor using a pinch valve at the liquid outlet, thus maintaining a continuous liquid flow in the reactor. All components of the experimental setup and the reactor were made of glass or 'teflon' or 'stainless' steel so that there was no ozone demand from corrosion of experimental setup components.

3. Model development

The model pertains to the tall cylindrical column of uniform cross-sectional area being used as a bubble contactor for contacting a gas mixture containing oxygen and ozone with water in the counter-current mode. Gas is applied at the bottom of the reactor as bubbles. Gas bubbles move upwards through the reactor, while water added from the top travels downwards. The objective is to describe the ozone concentration profile in the gas and liquid phase along the reactor height.

Assumptions made during the model development were as follows; the gas phase is considered to be plug flow, i.e., mass transport of the gas phase due to dispersion is neglected. The physical significance of this assumption is that gas bubbles input to the column at different times do not collide and coalesce during their rise through the column. This is a probable occurrence if ε_l is large and gas bubbles introduced into the column at different times are of uniform size; also, ozone being a sparingly soluble gas, it is assumed that mass transfer resistance for ozone absorption is confined to the liquid side, and the mass transfer is per Lewis–Whitman two film theory. Then, rate of ozone mass transfer from gas to liquid phase,

$$R_{O_3} = K_L a\{[O_3]_l^s - [O_3]_l\} \quad (1)$$

where

$$[O_3]_l^s = S[O_3]_g \quad (2)$$

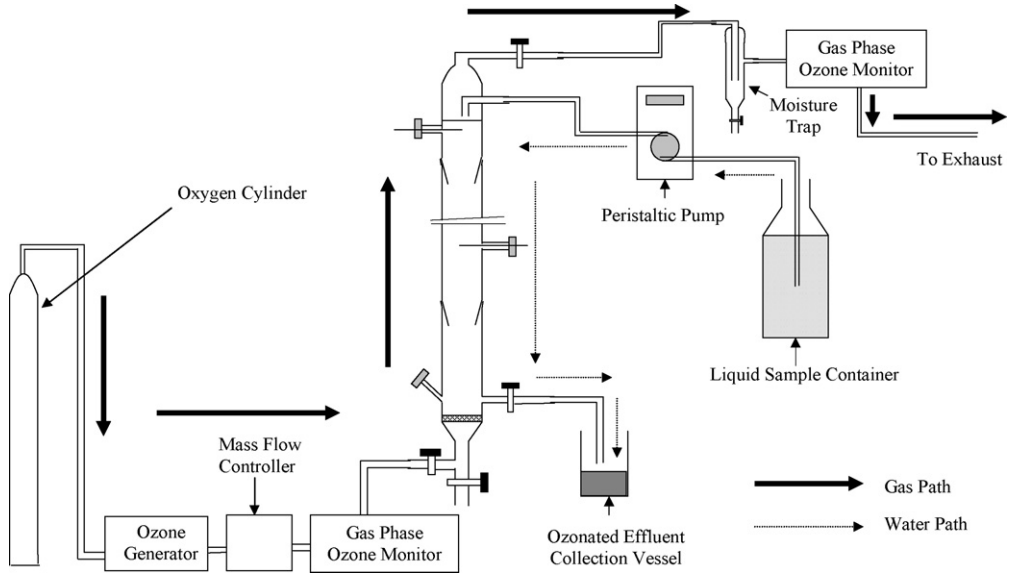

Fig. 2. Schematic of the experimental setup.

It is also assumed that net mass transfer of gaseous oxygen in the reactor to the liquid phase is zero, i.e., $Q_g[O_2]_g = \text{constant}$, all through the column height. This is a valid assumption if the water to be ozonated is saturated with oxygen. Then considering, $AU_g = Q_g$ and $[O_2]_g = P_{O_2} M_{O_2}/RT$,

$$P_{O_2} U_g = \text{constant} \tag{3}$$

where $P_{O_2} = P(1-y)$ and $P = P_A + \rho g \varepsilon_l (H-x)$

At $x=0$, i.e., at the bottom of the column, $P = P^o = P_A + \rho g \varepsilon_l H$.

At, $x=H$, i.e., at the top of the column, $P = P_A$.

Applying Eq. (3) at the bottom and at any height x in the column,

$$U_g[P_A + \rho g \varepsilon_l (H-x)](1-y) = U_{go} P^o (1-y_o) \tag{4}$$

hence

$$U_g = \frac{U_{go} P^o (1-y_o)}{[P_A + \rho g \varepsilon_l (H-x)](1-y)} \tag{4a}$$

in Eq. (4a),

$$y_o = \frac{P^o_{O_3}}{P^o} = \frac{[O_3]^o_g RT}{M_{O_3} P^o} \tag{5}$$

and

$$y = \frac{P_{O_3}}{P^o} = \frac{[O_3]_g RT}{M_{O_3}[P_A + \rho g \varepsilon_l (H-x)]} \tag{6}$$

Finally, it is assumed that there is no gas phase or aqueous phase reactions involving ozone consumption occurring in the column. This assumption is valid if the aqueous phase is pure water maintained at low pH, when aqueous ozone self-decomposition is negligible.

Under the circumstances, the partial differential equation describing gas phase ozone concentration profile in the column is,

$$\frac{\partial [O_3]_g}{\partial t} = -\frac{1}{\varepsilon_g}\frac{\partial}{\partial x}([O_3]_g U_g) - \frac{1}{\varepsilon_g} R_{O_3} \tag{7}$$

where U_g is a function of x (see Eqs. (4a), (5) and (6), and, the partial differential equation describing liquid phase ozone concentration profile in the column is,

$$\frac{\partial [O_3]_l}{\partial t} = \frac{1}{\varepsilon_l} U_L \frac{\partial [O_3]_l}{\partial x} + \frac{1}{\varepsilon_l} D_L \frac{\partial [O_3]_l}{\partial x^2} + \frac{1}{\varepsilon_l} R_{O_3} \tag{8}$$

For solving Eqs. (7) and (8) simultaneously, two initial conditions and three boundary conditions are required. These are as follows:

Initial conditions:

1. At $t=0$, $[O_3]_g = 0$, at all x.
2. At $t=0$, $[O_3]_l = 0$, at all x.

Boundary conditions:

1. At $t>0$, $[O_3]_g = [O_3]^o_g$ at $x=0$.
2. At $t>0$, $d[O_3]_l/dx = 0$ at $x=0$.
3. At $t>0$, $d[O_3]_l/dx = -[U_L/D_L][O_3]_l$ at $x=H$.

The first boundary condition is applicable to Eq. (7), and implies that the influent gaseous ozone concentration at the bottom of the column is known as a function of time. The second and third boundary conditions apply to Eq. (8). The second boundary condition implies that all interactions involving aqueous ozone come to a complete halt as soon as the water leaves the column at $x=0$. The third boundary condition implies that there is no advective or dispersive transport of aqueous ozone across the top boundary (at $x=H$) of the reactor.

4. Simulation results

Aqueous and gaseous ozone profiles were simulated as a function of reactor height, starting from start of ozonation ($t=0$) to the time steady state was reached ($t \to \infty$) by numerically solving the model developed (Eqs. (1)–(8)) using a numerical partial differential equation solver PDESOL. The simulated profiles represent conditions where no aqueous phase ozone decomposition is expected, as is the case when the aqueous phase is at low pH.

The simulated ozone profiles are shown in Fig. 3. The simulation conditions are presented in the figure caption. From the start of ozonation, when $[O_3]_g$ was zero all along column height, a progressive increase in the gaseous ozone concentra-

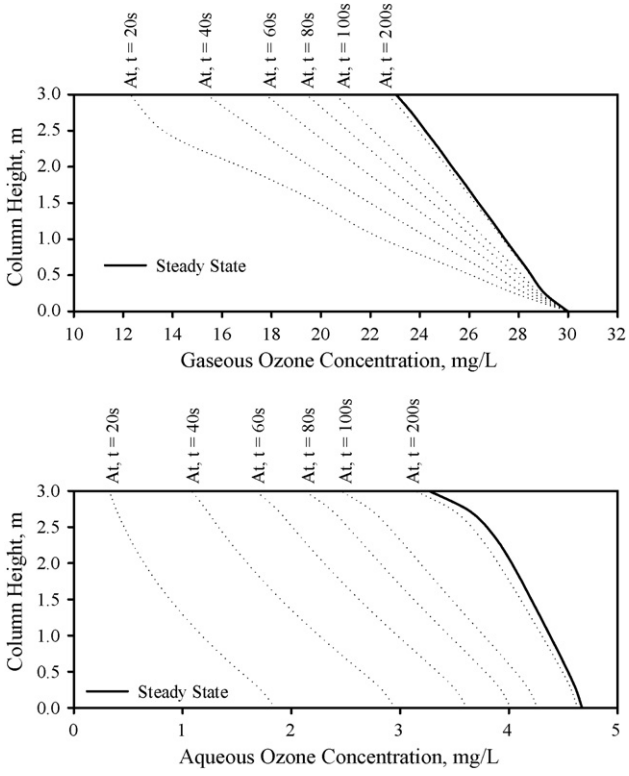

Fig. 3. Model simulation of gaseous and aqueous ozone profile in a counter-current ozone contactor. P^o: 130,730 Pa; P_A: 101,300 Pa; Q_g: 8.33×10^{-6} m^3 s^{-1}; T: 298 K; H: 3 m; Q_{go}: 6.46×10^{-6} m^3 s^{-1}; Q_l: 4.17×10^{-7} m^3 s^{-1}; A: 4.91×10^{-4} m^2; U_{go}: 1.32×10^{-2} m s^{-1}; S: 0.19; D_L: 1.37×10^{-3} m^2 s^{-1}; ε_g: 8.32×10^{-2}; $[O_3]^o_g$: 30 g m^{-3}; $K_L a = 0.025$ s^{-1}; R: 8.314 J mol^{-1} K^{-1}; M_{O_3}: 48 g mol^{-1}; ρ: 1000 kg m^{-3}; g: 9.81 m s^{-2}.

tion along column height is observed, until the steady state is reached. The steady state values decrease with increase in reactor height, since the gas phase expands with progressively lower pressure prevalent at higher reactor heights, leading to lowering in gaseous ozone concentration. Aqueous ozone profile also shows an increasing trend with time, until at steady-state the aqueous phase ozone concentration reaches the saturation value corresponding to the steady-state gaseous ozone concentration along most of the reactor height. However, at the very top of the reactor, where water with zero aqueous ozone concentration is continuously input, ozone mass transfer from gas to liquid phase continues even at steady state. Simulation results showing the temporal increase in gaseous and aqueous ozone concentration at various heights along the reactor are shown in Fig. 4. Results in both cases show that ozone concentration at all heights increase from zero initially to the steady-state value in case of both aqueous and gaseous ozone. The results further show that this attainment of steady state occurs quicker near the bottom of the reactor for both aqueous and gaseous ozone.

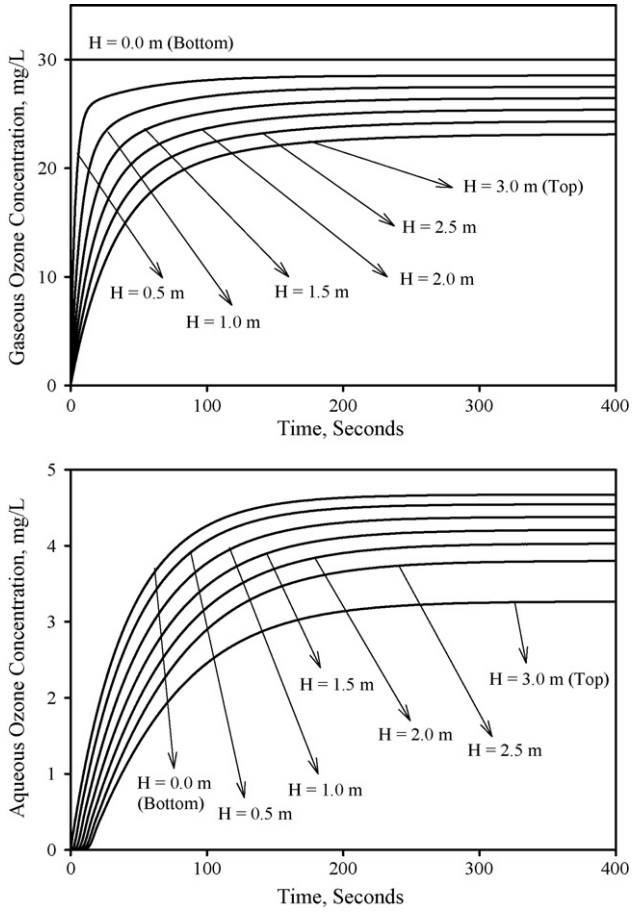

Fig. 4. Model simulation of the evolution of gaseous and aqueous ozone concentration in a counter-current ozone contactor at various heights. P^{o}: 130,730 Pa; P_A: 101,300 Pa; Q_g: 8.33×10^{-6} m^3 s^{-1}; T: 298 K; H: 3 m; Q_{go}: 6.46×10^{-6} m^3 s^{-1}; Q_l: 4.17×10^{-7} m^3 s^{-1}; A: 4.91×10^{-4} m^2; U_{go}: 1.32×10^{-2} m s^{-1}; S: 0.19; D_L: 1.37×10^{-3} m^2 s^{-1}; ε_g: 8.32×10^{-2}; $[O_3]_g^o$: 30 g m^{-3}; $K_La = 0.025$ s^{-1}; R: 8.314 J mol^{-1} K^{-1}; M_{O_3}: 48 g mol^{-1}; ρ: 1000 kg m^{-3}; g: 9.81 m s^{-2}.

5. Experimental procedures

5.1. Gas phase ozone decomposition

In order to check whether gaseous ozone concentration in the reactor is stable, ozone concentrations influent to and effluent from the reactor was monitored in the empty reactor under dry and 'steady-state' conditions at various voltage settings of the ozone generator and gas flow rates.

5.2. Gas hold-up

Gas hold-up, $\varepsilon_g = (1 - \varepsilon_L)$, was calculated by bubbling gas at different superficial velocities through the reactor containing water to an initial height of 3 m, and noting the increase in water level in the reactor due to entrainment of the gas bubbles.

5.3. Ozone contactor operation

All experiments involving the ozone contactor consisted of the following initial steps. First, oxygen flow was started at the desired rate by adjusting the MFC appropriately. The influent and effluent ozone concentration, as measured by the online ozone monitors was also set to zero at this time. Then, the reactor was filled up with water by employing the peristaltic pump in the 'fast' mode. Next, a continuous liquid flow at the desired rate was established through the reactor by adjusting the settings of the peristaltic pump in the influent end, and the pinch cork at the effluent end. Care was taken to ensure at this point that both gas and liquid flow rates through the reactor were steady and of the value desired. All experiments were carried out at a temperature of 30 °C, where the value of S was reported to be 0.16 [2].

5.4. Tracer studies for liquid phase dispersion coefficient determination

A typical tracer study for determination of the liquid phase dispersion coefficient in the ozone contactor involved addition of a 'slug' of methylene blue (6–8 mg) at the top of the reactor over a very short period of time. Concentration of methylene blue was measured at a sampling port, either 1 or 2 m below the column top, at various times after "slug" addition. Four milliliters of samples were collected from the sampling port for this purpose. Liquid flow rate (Q_l) during tracer experiments was either 10 or 25 mL min^{-1} (1.67×10^{-7} or 4.17×10^{-7} m^3 s^{-1}). Eight experiments (Experiments A–H) were carried out, four each at Q_g values of 500 and 1000 mL min^{-1} (8.33×10^{-6} to 1.67×10^{-5} m^3 s^{-1}), respectively (see Table 1 for details).

5.5. Mass transfer coefficient (K_La) determination

These experiments were carried out with pure water maintained at pH 3. Under these conditions, ozone decomposition in the aqueous phase was not expected. Continuous water and oxygen flow at predetermined rates was established as described earlier. Next, the ozonator was turned on. This resulted in the

Table 1
Conditions for dispersion experiments (Experiments A–H)

		$Q_l = 10\,mL\,min^{-1}$ ($1.67 \times 10^{-7}\,m^3\,s^{-1}$)		$Q_l = 25\,mL\,min^{-1}$ ($4.17 \times 10^{-7}\,m^3\,s^{-1}$)	
		$x = 2\,m$	$x = 1\,m$	$x = 2\,m$	$x = 1\,m$
Q_g[a] ($mL\,min^{-1}$)	500	Experiment A	Experiment B	Experiment C	Experiment D
	1000	Experiment E	Experiment F	Experiment G	Experiment H

[a] $500\,mL\,min^{-1} = 8.33 \times 10^{-6}\,m^3\,s^{-1}$; $1000\,mL\,min^{-1} = 1.66 \times 10^{-5}\,m^3\,s^{-1}$.

Table 2
Conditions for experiments for determining ozone mass transfer coefficient (Experiment Nos. 1–6)

		$Q_g = 500\,mL\,min^{-1}$ ($8.33 \times 10^{-6}\,m^3\,s^{-1}$)		
		$x = 1.5\,m$	$x = 2.0\,m$	$x = 2.5\,m$
Q_l[a] ($mL\,min^{-1}$)	10	Experiment No. 1	Experiment No. 2	Experiment No. 3
	25	Experiment No. 4	Experiment No. 5	Experiment No. 6

[a] $10\,mL\,min^{-1} = 1.67 \times 10^{-7}\,m^3\,s^{-1}$; $25\,mL\,min^{-1} = 4.17 \times 10^{-7}\,m^3\,s^{-1}$.

increase of gaseous ozone concentration influent to the reactor, as recorded by the ozone monitor, from zero to an increased, but approximately constant value. The effluent gaseous ozone concentration from the reactor and aqueous ozone concentrations at sampling ports (either at 1.5, 2.0 or 2.5 m from bottom) were also recorded with time. For measuring aqueous ozone concentration, a volume of liquid sample was extracted from a sampling port using a syringe and transferred into a 100 mL measuring flask containing indigo trisulfonate solution. Based on the collected data, value for K_La could be determined. Six experiments were carried out, three each at liquid flow rates (Q_l) of 10 and 25 $mL\,min^{-1}$ (1.67×10^{-7} or $4.17 \times 10^{-7}\,m^3\,s^{-1}$), respectively. Gas flow rate (Q_g) during all above experiments was $500\,mL\,min^{-1}$ ($8.33 \times 10^{-6}\,m^3\,s^{-1}$) (see Table 2 for details).

6. Analytical methods

Aqueous ozone was measured by the Indigo method [31,32], with the final absorbance of Indigo solution being measured spectrophometrically (Systronics 106, India) using a 4 cm path length quartz absorbance cell. In some cases, where interference was not expected, aqueous ozone concentration was directly measured by determining the UV absorbance of the aliquot containing aqueous ozone at 260 nm using a UV spectrophotometer (Cary 50 Conc., Varian) equipped with 1 cm absorbance cell (Borosil). Multiplication of this value by a factor of 14.59 [2] gave the ozone concentration in $mg\,L^{-1}$. Gaseous ozone was directly measured using an UV absorbance based ozone-monitoring device (ANSEROS, Ozomat GM-

Table 3
Gaseous ozone concentrations recorded at the inlet and outlet to the empty reactor

Ozonator power (percent of full power)	Inlet gaseous ozone concentration ($mg\,L^{-1}$)	Outlet gaseous ozone concentration ($mg\,L^{-1}$)	Percent difference in average values
Gas flow rate: $500\,mL\,min^{-1}$			
0	0.0	0.0	–
20	55.7 ± 0.61	54.8 ± 0.42	1.61
40	87.3 ± 3.06	86.4 ± 3.06	1.03
60	98.4 ± 1.86	97.4 ± 1.91	1.02
80	102.4 ± 4.03	101.4 ± 4.03	0.98
100	100.4 ± 3.26	99.5 ± 3.16	0.90
Gas flow rate: $750\,mL\,min^{-1}$			
0	0.0	0.0	–
20	39.2 ± 4.47	38.5 ± 4.72	1.78
40	70.3 ± 4.60	69.1 ± 4.80	1.71
60	80.9 ± 5.17	79.8 ± 5.46	1.36
80	94.2 ± 5.46	93.0 ± 5.50	1.27
100	94.5 ± 4.54	93.5 ± 4.50	1.06
Gas flow rate: $1000\,mL\,min^{-1}$			
0	0.0	0.0	–
20	36.8 ± 3.11	36.1 ± 2.80	1.74
40	68.8 ± 4.16	67.5 ± 4.26	1.89
60	83.4 ± 4.48	82.0 ± 4.65	1.61
80	93.2 ± 2.26	92.2 ± 2.29	1.10
100	95.3 ± 2.06	93.9 ± 2.29	1.44

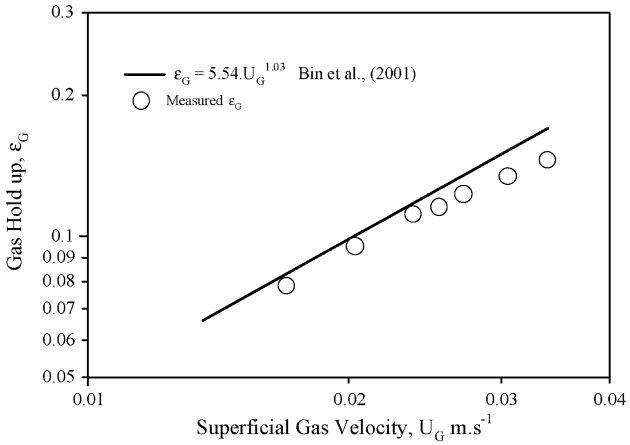

Fig. 5. Gas hold-up various Q_g values.

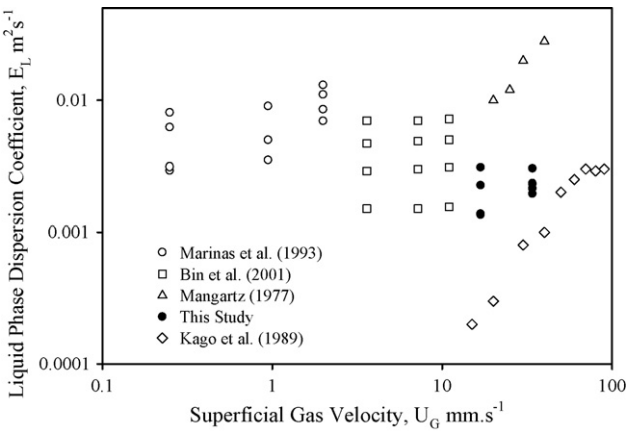

Fig. 6. Comparison of liquid phase dispersion coefficient values (D_L) obtained in this study with data from other sources.

6000-OEM, Germany). Absorbance scan using the Varian Cary 50 Conc. Spectrophotometer and an absorbance cell of 1 cm path length showed that the maximum absorbance of methylene blue was at 665 nm. Accordingly methylene blue aliquots of various concentrations were prepared and the absorbance values of these standards were measured to obtain a calibration curve for tracer studies. The concentrations of methylene blue in the experimental samples collected were determined as per the prepared calibration curve. pH was measured using a combination pH electrode (Toshniwal CL-51, India) connected to a digital pH meter (TOSCHCON CL-54, India).

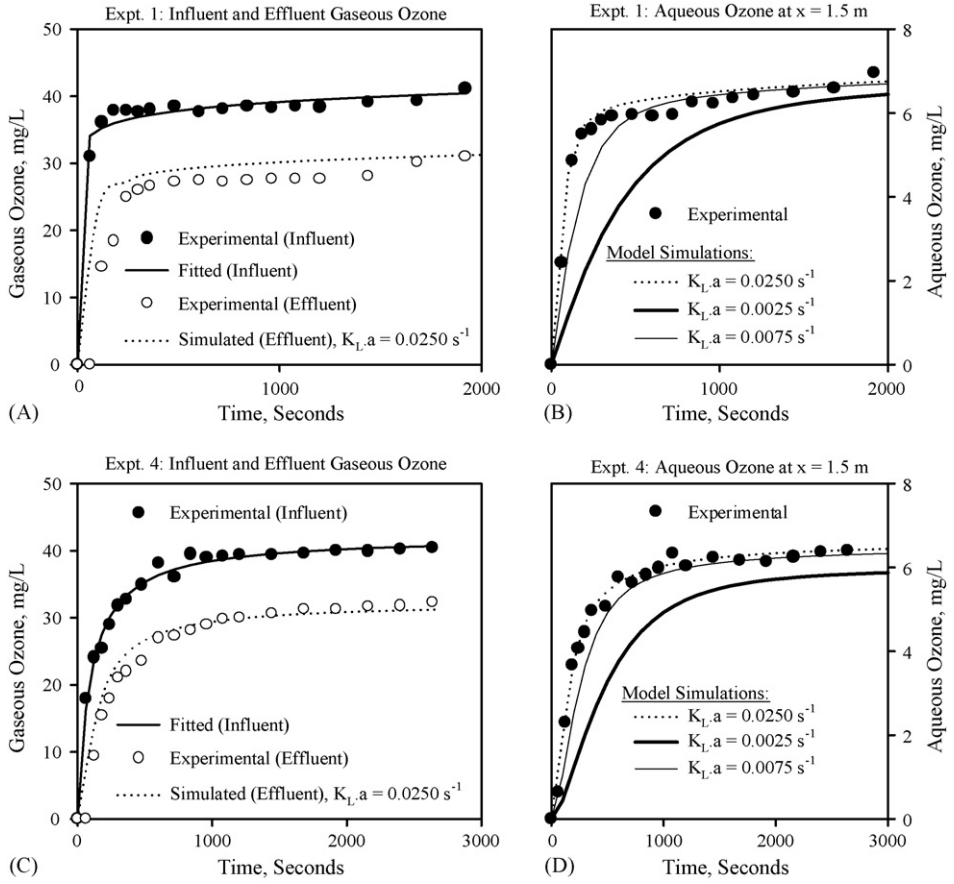

Fig. 7. Effluent gaseous ozone concentration and evolution of aqueous ozone concentration at $x = 1.5$ m: comparison of model simulation at three $K_L a$ values and experimental data. Experiment No. 1: Q_l: 1.67×10^{-7} m^3 s^{-1}; Experiment No. 4: Q_l: 4.17×10^{-7} m^3 s^{-1}; P^o: 130,730 Pa; P_A: 101,300 Pa; Q_g: 8.33×10^{-6} m^3 s^{-1}; T: 303 K; H: 3 m; Q_{go}: 6.56×10^{-6} m^3 s^{-1}; A: 4.91×10^{-4} m^2; U_{go}: 1.34×10^{-2} m s^{-1}; S: 0.16; D_L: 2.02×10^{-3} m^2 s^{-1}; ε_g: 8.32×10^{-2}; $[O_3]_g^o$: as per details in Table 4; g: 9.81 m s^{-2}; M_{O_3}: 48 g mol^{-1}; R: 8.314 J mol^{-1} K^{-1}; ρ: 1000 kg m^{-3}; aqueous pH: 3.0.

7. Results and discussion

7.1. Gas phase ozone decomposition

Influent and effluent gaseous ozone concentration to the empty reactor was measured and is summarized in Table 3. The results indicate that at all the three gas flow rates investigated, the difference between the influent and effluent gaseous ozone concentration was statistically insignificant. These results suggest that gaseous ozone is stable over the time periods of interest in this research.

7.2. Gas hold-up

Gas hold-up values were determined experimentally in the gas flow rate range of 500–1000 mL min^{-1}. As seen in Fig. 5, the experimental results are in broad agreement with the regression relationship developed by Biń et al. [5], relating gas hold-up with superficial gas velocity.

7.3. Liquid phase dispersion coefficient

Based on data obtained from tracer studies, liquid phase dispersion coefficient (D_L) was calculated corresponding to all eight experiments that were carried out. The procedure used for this purpose is as described in Biń et al. [5]. The average D_L value for the four experiments (A–D) carried out at Q_g of 500 mL min^{-1} (8.33×10^{-6} m^3 s^{-1}) was $(2.02 \pm 0.83) \times 10^{-3}$ while the corresponding average value for the experiments (E–H) carried out at Q_g of 1000 mL min^{-1} (1.66×10^{-5} m^3 s^{-1}) was $(2.34 \pm 0.46) \times 10^{-3}$ m^2 s^{-1}. The values obtained during our study have been compared with values of D_L reported by other researchers (see Fig. 6). The values obtained in this study are seen to be in general agreement with the values obtained by other researchers.

7.4. Estimation of ozone mass transfer coefficient

Ozone mass transfer coefficient, K_La, was estimated through comparison of model simulation results at various K_La values with the experimentally observed results. For simulation purposes, influent gaseous ozone concentration measured during the experiments (Experiment Nos. 1–6) were expressed as a function of time as shown in Table 4. This kind of representation was necessary for continuous specification of gaseous ozone concentration at $x = 0$, as a boundary condition for the associated PDE (see Eq. (7)). Simulation of aqueous ozone concentration was performed at Q_g value of 500 mL min^{-1} (8.33×10^{-6} m^3 s^{-1})

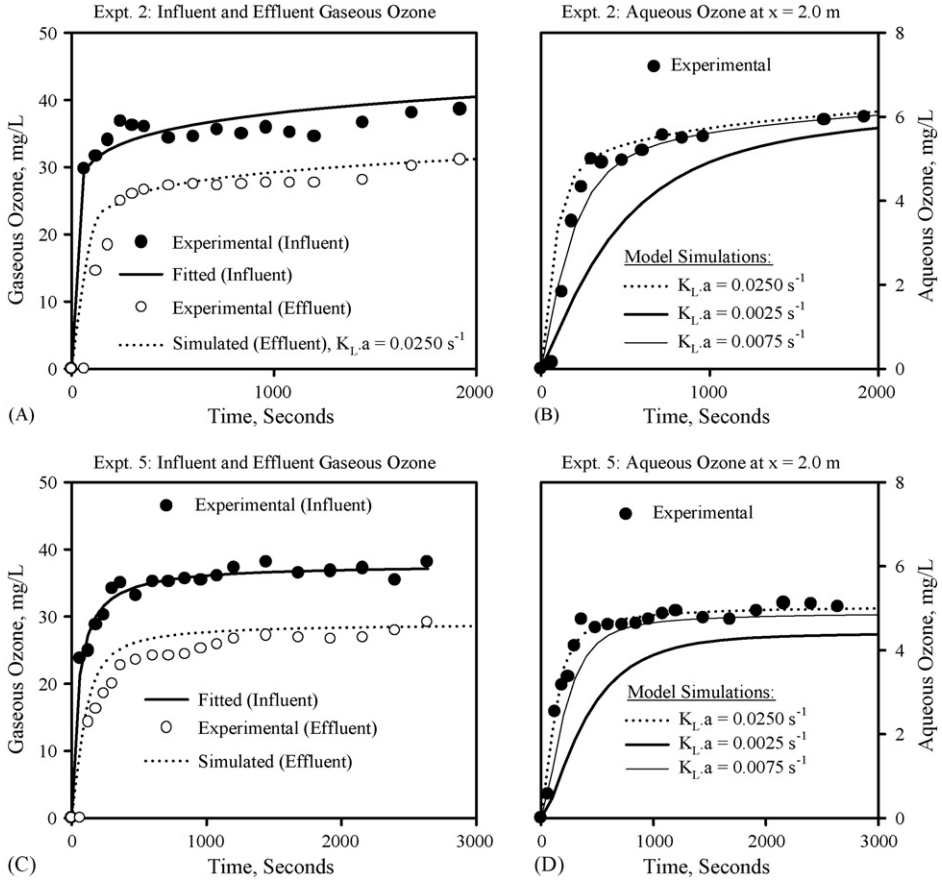

Fig. 8. Effluent gaseous ozone concentration and evolution of aqueous ozone concentration at $x = 2.0$ m: comparison of model simulation at three K_La values and experimental data. Experiment No. 2: Q_l: 1.67×10^{-7} m^3 s^{-1}; Experiment No. 5: Q_l: 4.17×10^{-7} m^3 s^{-1}; P^o: 130,730 Pa; P_A: 101,300 Pa; Q_g: 8.33×10^{-6} m^3 s^{-1}; T: 303 K; H: 3 m; Q_{go}: 6.56×10^{-6} m^3 s^{-1}; A: 4.91×10^{-4} m^2; U_{go}: 1.34×10^{-2} m s^{-1}; S: 0.16; D_L: 2.02×10^{-3} m^2 s^{-1}; ε_g: 8.32×10^{-2}; $[O_3]_g^o$: as per details in Table 4; g: 9.81 m s^{-2}; M_{O_3}: 48 g mol^{-1}; R: 8.314 J mol^{-1} K^{-1}; ρ: 1000 kg m^{-3}; aqueous pH: 3.0.

Table 4
Regression equations for describing influent gaseous ozone concentration to the reactor as a function of time

$Q_l = 10\ mL\ min^{-1}$ [a], $Q_g = 500\ mL\ min^{-1}$ [b]	$[O_3]_g\big\|_{x=0} = A(t)^B$, t = time in seconds		$Q_l = 25\ mL\ min^{-1}$ [c], $Q_g = 500\ mL\ min^{-1}$ [b]	$[O_3]_g\big\|_{x=0} = A(t)/(B+t)$, t = time in seconds	
	A	B		A	B
Experiment No. 1	27.84	0.049	Experiment No. 4	42.15	95.65
Experiment No. 2	20.30	0.091	Experiment No. 5	37.77	46.62
Experiment No. 3	24.32	0.064	Experiment No. 6	48.68	9.10

[a] $10\ mL\ min^{-1} = 1.67 \times 10^{-7}\ m^3\ s^{-1}$.
[b] $500\ mL\ min^{-1} = 8.33 \times 10^{-6}\ m^3\ s^{-1}$.
[c] $25\ mL\ min^{-1} = 4.17 \times 10^{-7}\ m^3\ s^{-1}$.

and for K_La values of 0.025, 0.0075 and 0.0025 s^{-1}. The experimental values of liquid phase dispersion coefficients and gas hold-up values determined earlier were used in these simulations. The experimental data and simulation results as described above for Experiment Nos. 1 and 4 are presented in Fig. 7. Similar results for Experiment Nos. 2, 5 are presented in Fig. 8, and for Experiment Nos. 3 and 6 are presented in Fig. 9. These results, taken as a whole, indicate that the simulation results corresponding to K_La value of 0.025 s^{-1} agree adequately with the experimental data in all six cases. This is irrespective of the liquid flow rate or the location of the sampling port where the determination was made. Comparison of the observed K_La value with regression relationships proposed for similar columns by various researchers is shown in Fig. 10. The K_La value reported in this study is seen to be in general agreement with the results published by other researchers. The K_La values determined by various researchers, as depicted in Fig. 10, are seen to vary by almost an order of magnitude even at the same superficial velocity. This variation may be attributed to variations in temperature, ionic strength of the liquid phase and most importantly, to variations in gas bubble size influent to the reactors. Everything else remaining the same, a smaller bubble size will result in a larger value of the mass transfer coefficient.

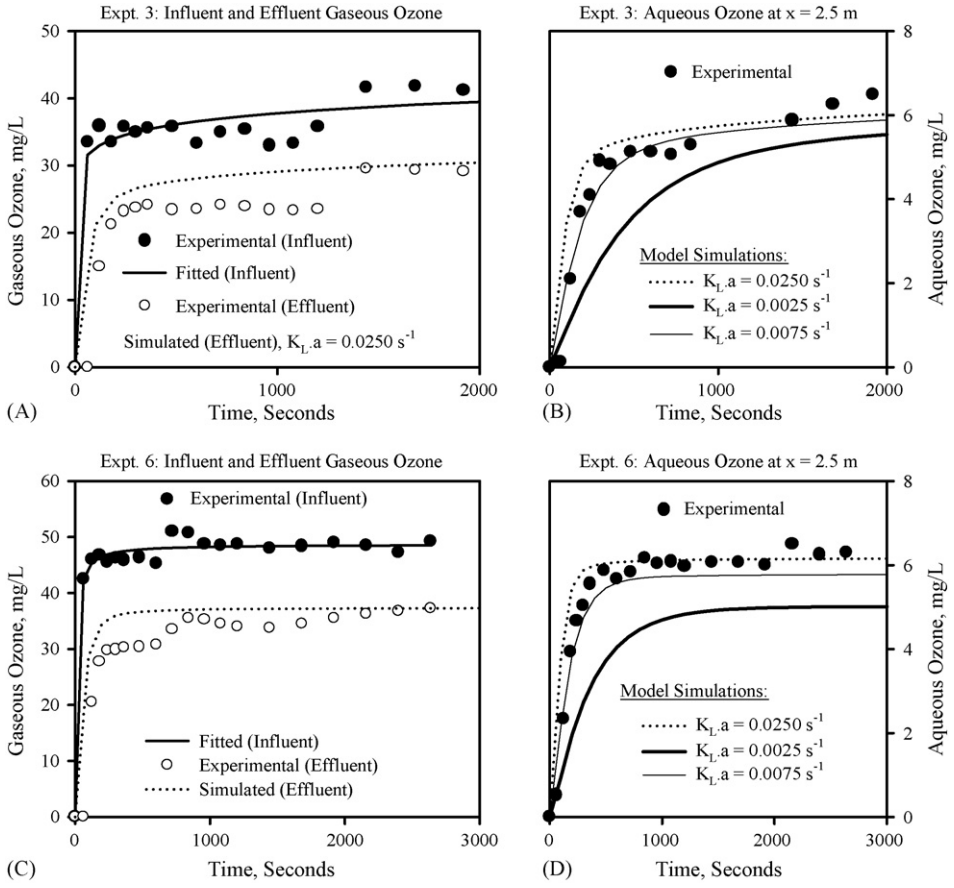

Fig. 9. Effluent gaseous ozone concentration and evolution of aqueous ozone concentration at $x = 2.5$ m: comparison of model simulation at three K_La values and experimental data. Experiment No. 3: Q_l: $1.67 \times 10^{-7}\ m^3\ s^{-1}$; Experiment No. 6: Q_l: $4.17 \times 10^{-7}\ m^3\ s^{-1}$; P^o: 130,730 Pa; P_A: 101,300 Pa; Q_g: $8.33 \times 10^{-6}\ m^3\ s^{-1}$; T: 303 K; H: 3 m; Q_{go}: $6.56 \times 10^{-6}\ m^3\ s^{-1}$; A: $4.91 \times 10^{-4}\ m^2$; U_{go}: $1.34 \times 10^{-2}\ m\ s^{-1}$; S: 0.16; D_L: $2.02 \times 10^{-3}\ m^2\ s^{-1}$; ε_g: 8.32×10^{-2}; $[O_3]_g^o$: as per details in Table 4; g: 9.81 $m\ s^{-2}$; M_{O_3}: 48 $g\ mol^{-1}$; R: 8.314 $J\ mol^{-1}\ K^{-1}$; ρ: 1000 $kg\ m^{-3}$; aqueous pH: 3.0.

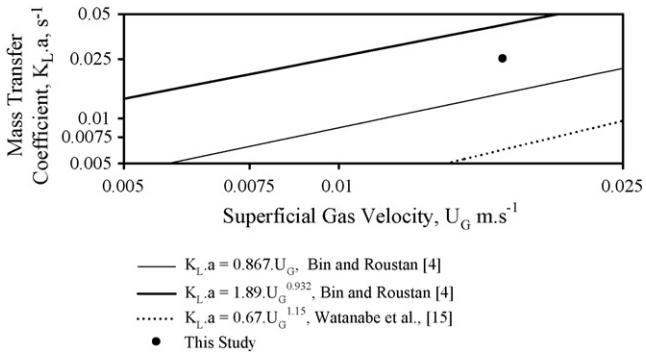

Fig. 10. Comparison of mass transfer coefficient value (K_La) determined in this study with results reported by other researchers.

7.5. Effluent gaseous ozone concentration

Model simulations with K_La value of 0.025 s^{-1} and influent gaseous ozone concentrations as specified in Table 4, also results in prediction of effluent gaseous ozone concentration as a function of time. Comparison of the experimentally observed effluent gaseous ozone concentration in Experiments 1–6 with the corresponding simulated values are also shown in Figs. 7–9. The experimental and simulated values are seen to match adequately in all cases. This can be considered as additional evidence in support of the correctness of the determined K_La value.

7.6. Sensitivity analysis

In addition to simulation runs carried out at K_La values of 0.025, 0.0075 and 0.0025 s^{-1}, additional simulations were also carried out at K_La values of 0.015 and 0.035 s^{-1} (results not shown) in each case. In all cases, visual comparison of simulations at K_La values of 0.015, 0.025 and 0.035 s^{-1} with corresponding experimental aqueous and gaseous ozone data showed adequate agreement. However, least square error between simulation results corresponding to K_La of 0.025 s^{-1} and the corresponding experimental aqueous and gaseous ozone data was the lowest in all cases.

8. Summary and conclusions

Characterization of a tall counter-current bubble type ozone contactor, which involves determination of gas phase hold-up (ε_g), liquid phase dispersion coefficient (D_L), and ozone mass transfer coefficient (K_La), has been described. The procedure used for determination of K_La is novel, and involves comparison of experimental data on evolution of aqueous phase ozone concentration at various heights in the contactor after start of ozonation with corresponding model simulation results. The value of K_La was determined by this procedure to be 0.025 s^{-1} at a superficial gas velocity (U_G) of 0.017 m s^{-1}. This value was in general agreement with results published by other researchers. The experimental data on evolution of effluent gaseous ozone concentration from the reactor operation under various conditions also matched well with corresponding simulation results, suggesting correctness of the determined K_La value. Sensitivity analysis indicated that the model simulation results were relatively insensitive to changes in K_La value in the range of 0.015–0.035 s^{-1}.

The model described here for determination of K_La value may be considered a building block for more complex models for describing, (1) ozone self-decomposition in pure water containing known promoters/scavengers, (2) ozone decomposition and degradation of micro-pollutants in pure water which contains known promoters/scavengers, or, (3) ozone decomposition and degradation of micro-pollutants in the natural waters containing poorly characterized background organic and inorganic contaminants. Work in these areas are currently undergoing in our laboratory and elsewhere.

References

[1] J.L. Sotelo, F.J. Beltran, M. Gonzalez, J. Dominguez, Effect of high salt concentrations on ozone decomposition in water, J. Environ. Sci. Health A24 (1989) 823.
[2] B. Langlais, D.A. Reckhow, D.R. Brink (Eds.), Ozonation in Water Treatment. Applications and Engineering. Cooperative Research Report. AWWRF and Compagnie Generale des Eaux, Lewis Publishers, 1991.
[3] F.J. Beltran, J.F. Garcia-Araya, J.M. Encinar, Henry and mass transfer coefficients in ozonation of wastewater, Ozone Sci. Eng. 19 (1997) 281.
[4] A.K. Biń, M. Roustan, Mass transfer in ozone reactors, in: Proceedings of the International Specialised Symposium IOA 2000 "Fundamental and Engineering Concepts for Ozone Reactor Design", Toulouse, March 1–3, 2000, pp. 99–131.
[5] A.K. Biń, B. Duczmal, P. Machniewski, Hydrodynamics and ozone mass transfer in a tall bubble column, Chem. Eng. Sci. 56 (21/22) (2001) 6233–6240.
[6] A.K. Biń, Ozone dissolution in aqueous systems. Treatment of the experimental data, Exp. Therm. Fluid Sci. 28 (2004) 395–405.
[7] M. Bouaifi, G. Hebrard, D. Bastoul, M. Roustan, A comparative study of gas hold-up, bubble size, interfacial area and mass transfer coefficients in stirred gas-liquid reactors and bubble columns, Chem. Eng. Process. 40 (2) (2001) 97–111.
[8] E.S. Gaddis, Mass transfer in gas–liquid contactors, Chem. Eng. Process. 38 (4–6) (1999) 503–510.
[9] P.R. Gogate, A.B. Pandit, Survey of measurement techniques for gas–liquid mass transfer coefficient in bioreactors, Biochem. Eng. J. 4 (1) (1999) 7–15.
[10] G. Hebrard, D. Bastoul, M. Roustan, Influence of the gas sparger on the hydrodynamic behaviour of bubble columns, Trans. Inst. Chem. Eng. 74 (A3) (1996) 406–414.
[11] T. Kago, Y. Sasaki, T. Kondo, S. Morooka, Y. Kato, Gas holdup and axial dispersion of gas and liquid in bubble columns of homogeneous bubble flow regime, Chem. Eng. Commun. 75 (1989) 23–38.
[12] M. Kuosa, A. Laari, J. Kallas, Determination of the Henry's coefficient and mass transfer for ozone in a bubble column at different pH values of water, Ozone Sci. Eng. 26 (3) (2004) 277–286.
[13] H.M. Letzel, J.C. Schouten, R. Krishna, C.M. van den Bleek, Gas holdup and mass transfer in bubble column reactors operated at elevated pressure, Chem. Eng. Sci. 54 (13/14) (1999) 2237–2246.
[14] K. Petera, P. Ditl, Effect of pressure profile on evaluation of volumetric mass transfer coefficient K_La in bioreactors, Biochem. Eng. J. 5 (1) (2000) 23–27.
[15] K. Watanabe, I. Kinugasa, K. Higaki, Ozone absorption in bubble column, Memoir Niihama Natl. College Technol. 27 (1991) 48–52.
[16] N. Le Sauze, A. Laplanche, N. Martin, G. Martin, Modeling ozone transfer in a bubble column, Water Res. 27 (1993) 1071.
[17] H. Zhou, D.W. Smith, S.J. Stanley, Modeling dissolved ozone concentration profiles in bubble columns, J. Environ. Eng., ASCE 120 (1994) 821.
[18] M.G. El-Din, Theoretical Analysis and Experimental Investigation of the Performance of Ozone Bubble Columns, Ph.D. Thesis, University of Alberta, 2001.

[19] B.J. Mariñas, S. Liang, E.A. Aieta, Modeling hydrodynamics and ozone residual distribution in a pilot-scale ozone bubble-diffuser contactor, J. Am. Waterworks Assoc. 85 (3) (1993) 90–99.
[20] K. Muroyama, T. Norieda, A. Morioka, T. Tsuji, Hydrodynamics and computer simulation of an ozone oxidation reactor for treating drinking water, Chem. Eng. Sci. 54 (21) (1999) 5285–5292.
[21] M.G. El-Din, D.W. Smith, Designing ozone bubble columns: a spreadsheet approach to axial dispersion model, Ozone Sci. Eng. 23 (2001) 369.
[22] J.-H. Kim, R.B. Tomiak, B.J. Marinas, Inactivation of *Cryptosporidium* oocysts in a pilot-scale ozone bubble-diffuser contactor. I. Model development, J. Environ. Eng., ASCE 128 (2002) 514.
[23] Y. Qiu, Kinetic and Mass Transfer Studies of the Reactions Between Dichlorophenols and Ozone in Liquid–Liquid and Gas–Liquid systems, Ph.D. Thesis, Mississippi State University, 1999.
[24] F.J. Beltran, J.F. Garcia-Araya, V. Navarrete, F.J. Rivas, An attempt to model the kinetics of the ozonation of simazine in water, Ind. Eng. Chem. Res. 41 (2002) 1723.
[25] F.J. Beltran, M. Gonzalez, B. Acedo, J. Rivas, Use of the axial dispersion model to describe the O_3 and O_3/H_2O_2 advanced oxidation of alachlor in water, J. Chem. Technol. Biotechnol. 77 (2002) 584.
[26] M. Hautaniemi, J. Kallas, R. Munter, M. Trapido, Modeling of chlorophenol treatment in aqueous solutions. 1. Ozonation and ozonation combined with UV radiation under acidic conditions, Ozone Sci. Eng. 20 (1998) 259.
[27] M. Hautaniemi, J. Kallas, R. Munter, M. Trapido, A. Laari, Modeling of chlorophenol treatment in aqueous solution. 2. Ozonation under basic conditions, Ozone Sci. Eng. 20 (1998) 283.
[28] Ch.S. Hull, Modelling of ozone contactors, Ph.D. Thesis, University of North Carolina, 1995.
[29] P.-C. Chiang, Y.-W. Ko, C.-H. Liang, E.-E. Chang, Modeling an ozone bubble column for predicting disinfection efficiency and control of DBP formation, Chemosphere 39 (1) (1999) 55–70.
[30] J.A. Pedit, K.J. Iwamasa, C.T. Miller, W.H. Glaze, Development and application of a gas–liquid contactor model to simulate advanced oxidation process, Environ. Sci. Technol. 31 (1998) 2791.
[31] APHA, AWWA, WPCF, Standard Method for Examination of Water and Wastewater, 19th ed., APHA, Washington, DC, 1995.
[32] H. Bader, J. Hoigne, Determination of ozone in water by indigo method, Water Res. 15 (1981) 449.